# MCF Skew Estimation at the Receiver for ARoF Antenna Beamforming

Thomas Nikas, Evangelos Pikasis, Sotiris Karabetsos, Dimitris Syvridis

# MCF Skew Estimation at the Receiver for ARoF Antenna Beamforming

Thomas Nikas[1[0000-0003-2501-0777]], Evangelos Pikasis[2], Sotiris Karabetsos[3[0000-0002-6454-5152]], and Dimitris Syvridis[1]

[1] Dept. of Informatics and Telecommunications, National and Kapodistrian University of Athens, Athens, GR-15784, Greece
[2] Eulambia Advanced Technologies Ltd., GR-15342, Ag. Paraskevi, Greece
[3] Dept. of Electrical and Electronics Engineering, University of West Attika, Egaleo, GR-12241 Greece
tnikas@di.uoa.gr

**Abstract.** Multicore fibers can be used for Radio over Fiber transmission of mmwave signals for phased array antennas in 5G networks. The inter-core skew of these fibers distorts the radiation pattern and has to be measured and compensated. We propose a method to accurately measure the differential delays remotely, after installation, without intervening heavily with the transmitter set-up. The properties of the phase response measured at a distant receiver are exploited to acquire the differential delays among the antenna array elements.

**Keywords:** Multicore Fiber, Inter-core skew, Radio over fiber, Phased arrays, Beam steering

## 1 Introduction

Antenna beam forming is adopted in a wide area of radio applications and recently in 5G wireless technology. In 5G, coverage and bandwidth requirements push the operating frequencies to mmwave, deploying dense pico- and femto-cell networks [1]. Orthogonal Frequency Division Modulation (OFDM) with its variants is the most prominent modulation scheme proposed for 5G [2]. Beam-forming (BF) is utilized to alleviate the free space path loss and through wall attenuation, important factors for efficient radio coverage at mmwave frequencies. Base station to vehicle communication quality is also enhanced using a steerable beam that tracks the mobile user. Commonly, the phase shifting process takes place at the transmitter, just before power amplification and feeding of the individual antenna elements. Manufacturing tolerances, aging of components and temperature variations at outdoor installations generate phase alignment errors which distort the radiation pattern. Furthermore, the component phase responses and transmission line path lengths after the phase shifting stage must be identical in order to preserve the beam quality. These factors and requirements become more critical in higher operating frequencies and in a multi-beam

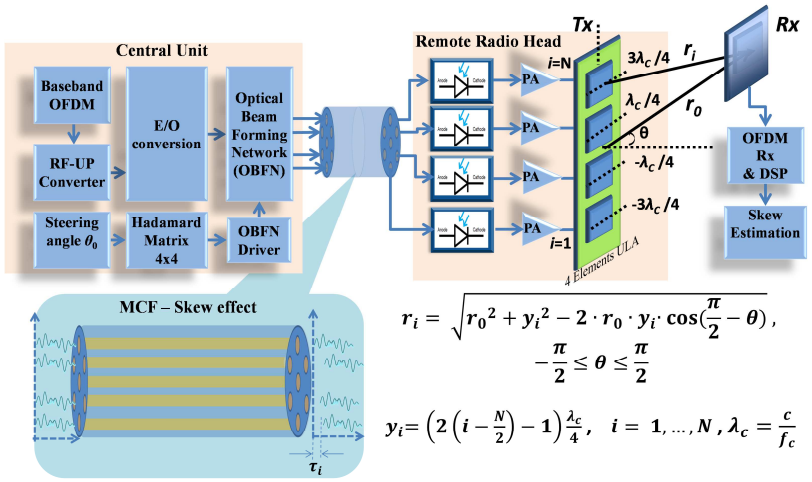


**Fig. 1.** The ARoF system with OBFN, MCF link, RRH with $N$=4 element, $\lambda_c/2$ spaced array and radio propagation model.

antenna, which is fed by some form of fixed or configurable phase shifting network, like Blass or Butler matrices.

A promising technique to serve network densification and flexible resource allocation in 5G is Radio over Fiber (RoF). The analog variant of RoF (ARoF) is especially suited for remote antenna beam forming. The phase shifting process can be performed using Optical Beam Forming Networks (OBFNs) which are True Time Delay (TDD) devices and provide squint free beams [3]. The OBFNs are preferably located at the Central Unit (CU) and multi-core fibers (MCFs) are used to convey the phase shifted optical signals to the Remote Radio Heads (RRHs) [4]. The RF modulated, phase shifted optical carriers are detected, amplified and feed the antenna array elements, greatly simplifying the RRHs. MCF fibers present both static and dynamic differential delays among the fiber cores [5], which must be equalized to prevent severe RF beam pattern distortion. The full equalization of the effective path lengths is cumbersome and energy inefficient, mainly involving manual calibration. An automatic partial equalization method has been proposed [6] in which the remainder modulo 2kπ of the differential phase shifts is equalized. In either case of full or partial equalization, the differential delays must be accurately measured and compensated.

The static inter-core skew can be measured with optical means, like time domain or correlation reflectometers [7] before fiber installation. Dynamic MCF skew and any additional differential delays due to optical connectors and electronic path inequalities in various points of the CU and RRH subsystems, as well as aging and manufacturing tolerances are not measured. These stray delays might be large enough to distort the antenna radiation pattern. On the other hand, it is preferable to characterize the RoF and RF transmission system as a whole, using a single method. Advanced techniques,

like pseudo-noise gating [8, 9] using orthogonal sequences have been proposed for satellite antenna beamforming alignment and characterization.

In this paper, we propose a novel method for measuring the differential delays among the antenna elements, emerged either from optical or electrical length inequalities or both. It is based on the OFDM frequency domain equalization process at the receiver and exploits the phase response of the acquired system transfer function to estimate each antenna element delay. The process is mainly performed on installation, as an initial calibration procedure, as well as at periodic maintenance periods, involving minimum modifications in standard OFDM transmitter and receiver. Moreover, it is tolerant to multipath propagation. The resolution of the measured delays depends on the bandwidth of the OFDM signal.

## 2 Theoretical Model

The architecture of the ARoF system is shown in fig. 1, depicting the model for the followed analysis. The baseband OFDM signal is formed using pilot QAM symbols known to the receiver in all used subcarriers, in order to acquire with maximum resolution the system transfer function. The baseband signal is then up-converted to the required radio frequency and modulates linearly the optical carrier. The OBFN imposes the appropriate phase shifts for steering the antenna beam and launches $N$ optical signals to $N$ cores of the MCF. At the RRH, each core feeds the corresponding photodiode and RF amplification chain leading to the antenna element. The antenna consists of $N$, $\lambda_c/2$ spaced elements, forming a uniform linear array (ULA). The inter-core skew imposes differential time delays $\tau_i$, $i$=1,..,$N$ to the signals arriving at RRH which have to be compensated partially or completely. At RRH, the $N$ photocurrents are expressed as $I(i,t) = I_{0,i} \cdot s(t-\tau_i) \cdot \mathrm{e}^{\mathrm{j}2\pi f_c t}$, $i = 1,..,N$ where $s(t-\tau_i)$ are the baseband OFDM signals delayed by $\tau_i$ per core, $I_{0,i}$ is the complex value of the $i$-th photocurrent and $I_{0,i} = \left|I_{0,i}\right| \mathrm{e}^{-\mathrm{j}(i-1)\pi \sin\theta_0}$. The phase delay step $\pi \sin\theta_0$ is imposed by the OBFN to steer the beam to $\theta_0$ and the amplitude of the photocurrent is set to $\left|I_{0,i}\right| = 1/\sqrt{N}$ using uniform excitation, normalized to unity power. At the receiver antenna located at distance $r_0$ and azimuthal angle $\theta_0$, the summation of the electrical fields produced by each antenna element is expressed as $E_R(t) = \sum_{i=1}^{N} aI_{0,i} s(t-\tau_\iota) e^{j2\pi f_c t}\, e^{-j2\pi f_c r_i/c}$, where $a$ is a factor expressing the linear relation of the electrical field and antenna current as well as line of sight path loss. The factor $a$ is assumed time invariant and frequency independent within the signal bandwidth.

After reception, analog to digital conversion and FFT, the received signal $R(t)$ is transformed to the discrete frequency domain $R_k = ab \sum_{i=1}^{N} I_{0,i} X_k e^{-j2\pi(f_c + k/T_S)\tau_i}\, e^{-j2\pi f_c r_i/c}$, where $X_k$, $R_k$ are the transmitted and received QAM pilot symbols of the k-th OFDM subcarrier and the factor $b$ expresses the linear electrical field – antenna current relation, assumed to have the same time invariability and frequency independence properties of a. Then, the discrete frequency domain transfer function is

$$H_k = \frac{R_k}{X_k} = ab \sum_{i=1}^{N} I_{0,i} e^{-j2\pi(f_c + k/T_S)\tau_i}\, e^{-j2\pi f_c r_i/c} \qquad (1)$$

As the receiver is located at the transmitter antenna far field $r_i \cong r_0 - y_i \cdot \sin\theta_0$(fig. 1) and taking into account the phase shifts imposed by the OBFN to steer the antenna main lobe to $\theta_0$, the transfer function is expressed as

$$H_k = \frac{ab}{\sqrt{N}} e^{-j[\frac{2\pi f_c r_0}{c} + \frac{\pi}{2}\cdot\sin\theta_0\cdot(N-1)]} \sum_{i=1}^{N} e^{-j2\pi(f_c + k/T_s)\tau_i} \quad (2)$$

Setting the constant terms $abe^{-j[\frac{2\pi f_c r_0}{c} + \frac{\pi}{2}\cdot\sin\theta_0\cdot(N-1)]}$, equal to unity, the transfer function becomes

$$H_k = \frac{1}{\sqrt{N}} \sum_{i=1}^{N} e^{-j2\pi(f_c + k/T_s)\tau_i} = \sum_{i=1}^{N} h_k^i \quad (3)$$

In (3), the complex value of $H_k$ in every OFDM subcarrier $k$ is the vector sum of the $h_k^i = \frac{1}{\sqrt{N}} e^{-j2\pi(f_c + k/T_s)\tau_i}$ terms, contributed from all $N$ transmitter antenna elements with various $\tau_i$ delays. The $h_k^i$ terms can be seen as the individual transfer functions at subcarrier $k$ from each transmitter antenna element $i$ to the receiver. The phase $-2\pi(f_c + k/T_s)\tau_i$ of $h_k^i$ as a function of $k$ is linear, with slope $-2\pi\tau_i/T_s$, from which the time delays $\tau_i$ can be calculated.

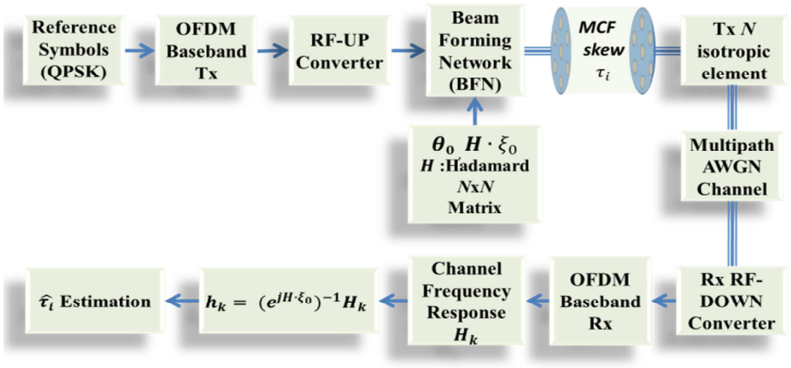


**Fig. 2.** The simulation model. The $\boldsymbol{H} \cdot \xi_0$ phase shifts are imposed via the BFN prior to MCF transmission.

The problem is to determine the individual element transfer function $h_k^i$ from the received sum in (3). For this reason, we impose additional, known to the receiver phase shifts $\xi_{i,m}$ via the beam forming network to every $m$-th OFDM symbol, $m = 1 \ldots N$, of $N$ successive symbols. Then, the transfer function for the $m$-th OFDM symbol in the time series of $N$ symbols is expressed as

$$H_{k,m} = \sum_{i=1}^{N} e^{j\xi_{i,m}} h_k^i \quad (4)$$

The phase shifts are set to $\xi_{i.m} = H_{i,m} \cdot \xi_0$, where $H_{i,m}$ are elements of a non-singular matrix $\boldsymbol{H}_{NxN}$ and $\xi_0$ is a constant. In matrix form, (4) is written as

$$\boldsymbol{H_k} = e^{j\boldsymbol{H}\cdot\xi_0} \boldsymbol{h_k} \quad (5)$$

In order to calculate $\boldsymbol{h_k}$ from the $N$ successive values of $\boldsymbol{H_k}$, we have to solve the

$N \cdot N$ linear system in (5) for all subcarriers. The matrix $e^{j\boldsymbol{H}\cdot\xi_0}$ must be invertible, so we choose $\boldsymbol{H}_{NxN}$to be a Hadamard matrix and $\xi_0 \neq \pi$. The obtained values for all MCF cores and antenna elements are

$$\boldsymbol{h_k} = (e^{j\boldsymbol{H}\cdot\xi_0})^{-1}\,\boldsymbol{H_k} \tag{6}$$

from which the time delays $\tau_i$ can be calculated. Recalling that the phase of $h_k^i$ as a function of k is linear, with a slope of $-\frac{2\pi\tau_i}{T_s} = -\omega_s\tau_i$, then the delays can be estimated as the mean value of $\angle h_{k+1}^i - \angle h_k^i$,

$$\widehat{\tau_i} = -\frac{\sum_{k=-\frac{N_{F_u}}{2}}^{\frac{N_{F_u}}{2}-1}\left(\angle h_{k+1}^i - \angle h_k^i\right)}{N_{F_u}\omega_s} \tag{7}$$

$N_{F_u}$being the number of the used OFDM subcarriers. Alternatively, the phase slope of $h_k^i$can be estimated by applying linear least squares regression to the $\varphi_k^i = \angle h_k^i$ samples. The $a$ (rad/Hz) coefficient of the fitted function

$$\widehat{\varphi_k^i} = a \cdot {}^{k}/_{T_s} + b, \qquad \widehat{\tau_i} = -a/2\pi \tag{8}$$

is the phase slope, while the constant term $b$ is the remainder modulo $2\pi$ of $-2\pi f_c\tau_i$. In this sense, the carrier frequency is not affecting the estimation process. On the contrary, wider signal bandwidth provides sufficient phase information both for the mean value estimation in (7) and the linear regression and is expected to influence the accuracy. This factor shall be further studied in the following section.

## 3 Numerical Analysis

In order to evaluate the proposed method, we performed simulations of ARoF, multi-path wireless and skew estimation systems. The simulation model is depicted in fig.2. At first, *N* successive baseband OFDM pilot symbols are generated and up-converted to the carrier frequency. Each time domain symbol is split to *N* identical streams and appropriate phase shifts for steering the main lobe to $\theta_0$ along with the $\xi_{i.m}$ phase offsets are applied by passing through the OBFN. The MCF skew delays are inserted to the *N* streams and the signals are transmitted to the multi-path radio channel. Gaussian white noise of variable power spectral density is added and the summation of electrical fields is calculated at the receiver antenna. After down-conversion and FFT, the system transfer functions $H_k$ for the *N* successive OFDM symbols are acquired. The linear system is solved using (6) and the time delays $\widehat{\tau_i}$ are calculated using (7) and (8). Then, the absolute estimation error $|\tau_i - \widehat{\tau_i}|$ is computed in both cases.

The simulation parameters are listed in table I, chosen so as to follow 5G New Radio numerology and beyond. The generated OFDM signal bandwidth is roughly 400 MHz centered at a carrier frequency of 26 GHz. The non-linearity of electro-optical conversion and photodiode shot noise contribution is not included in the model. Instead, the overall ARoF transmission, free space radio propagation and receiver noise figure are characterized by the final signal to noise ratio (SNR) at the receiver.

**Table 1.** Simulation Model Parameters

| Parameter | Value |
|---|---|
| Modulation per subcarrier | QPSK (4-QAM) |
| Sampling frequency Fs | 983.04 MHz |
| FFT/IFFT size NF | 4096 |
| Number of used subcarriers NFu | 416 - 2500 |
| OFDM symbol duration Ts (w/o CP) | 4.16us |
| Subcarrier spacing, 1/Ts | 240KHz |
| Cyclic Prefix (CP) | 520ns |
| Total symbol duration | 4.68 us |
| Signal bandwidth | 100 - 600 MHz |
| Carrier frequency fc | 26 GHz |
| Received signal SNR | 10 – 30 dB |
| Offset angle $\xi_0$ | π/2 rad |
| Azimuthal steering angle $\theta_0$ | 0° |
| Multipath delay | 80ns, 400ns |
| Multipath gain | -6dB, -20dB |
| Number of Tx antenna elements, N | 8, 16 |
| MCF skew delays, $\tau_i$ | Uniformly distributed, with maximum delay of 1 ns |

The multipath propagation model is static, not involving Doppler shift and comprises the strong line of sight component, which is dominant in higher microwave and mmwave frequencies. Except line of sight, two more propagation paths are considered, with relative to line of sight delays not exceeding the OFDM cyclic prefix. The offset angle $\xi_0$ was set to π/2 imposing ±π/2 phase offset, in order to achieve the maximum possible phase shift of π radians when multiplied with opposite sign elements of the Hadamard matrix. The inter-core differential delays of the MCF are uniformly distributed samples with maximum value of 1 ns. The receiver could be located at any known to the transmitter azimuthal angle $\theta_0$ and the beam forming network imposes the corresponding phase offsets to the antenna currents. These offsets do not affect the skew estimation as they are canceled out by the different propagation lengths from each transmitter element to the receiver. So, the beam steering angle $\theta_0$ was set to 0° supposing that the OFDM receiver is located at this azimuthal angle.

At first, a set of delays was inserted in the MCF transmission model for *N*=4 antenna elements and the proposed method was applied in the multipath radio propagation environment. The receiver SNR was set to 30 dB and the OFDM bandwidth to 400 MHz. The solution of the linear system $\boldsymbol{h_k} = (e^{j\boldsymbol{H}\cdot\xi_0})^{-1}\,\boldsymbol{H_k}$ provided the phase estimation per antenna element depicted in fig. 3, where the higher delay values result in steepest phase slope. The observed ripple is attributed to the multipath propagation.

Next, several random sets of skew delays for *N*=8 antenna elements are considered

in MCF transmission and estimated at the receiver with SNR of 20 dB and 400 MHz bandwidth, using both (7) and linear least squares regression (8). In all cases, the linear least squares regression performed better, minimizing the error between the estimated and actual delays. So, it is used throughout the following steps. Then, the offset angle $\xi_0$ was reduced from $\pi/2$ to $\pi/3$. The estimation error increased, attributed to the decreased phase shift among the BFN imposed phase values, $2\pi/3$ instead of $\pi$. So, the initial assumption that maximum phase shift offers the best possible accuracy is confirmed and used throughout the following simulations.

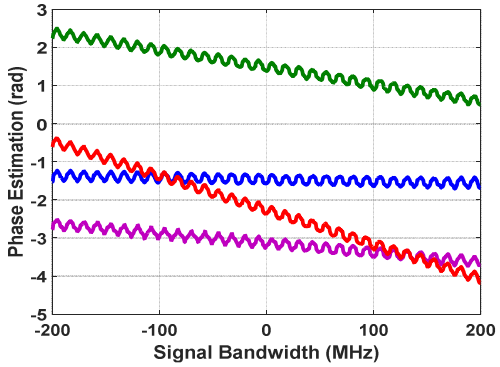


**Fig. 3.** The phase estimation per antenna element for $N$=4 for $\tau_1$=80 ps (blue), $\tau_2$=400 ps (purple), $\tau_3$=720 ps (green), $\tau_4$=1430 ps (red).

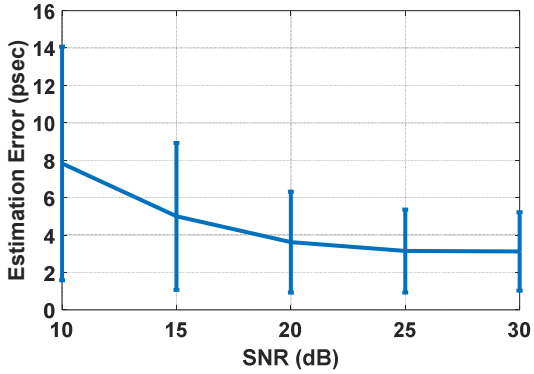


**Fig. 4.** The estimation error versus receiver SNR for $N$=8 antenna elements.

In order to evaluate the measurement resolution of the proposed scheme, 100 sets of skew delays for $N$=8 and $N$=16 transmitting antenna elements are considered and estimated with variable SNR at the receiver. The mean error between the estimated and actual delays as well as the associated standard deviation is calculated and the results for $N$=8 and $N$=16 elements are depicted in fig. 4 and fig. 5 respectively. The estimation error is converging to roughly 3 ps for SNR higher than 20 dB. This value

corresponds to 8% ambiguity compared to the period $1/f_c$ of the 26 GHz carrier frequency. Such a small value is not affecting the antenna radiation pattern, as will be confirmed in the following. For $N$=16 antenna elements (fig. 5), the estimation error is reduced for lower SNR and approaches the same value of roughly 3 ps for higher SNR.

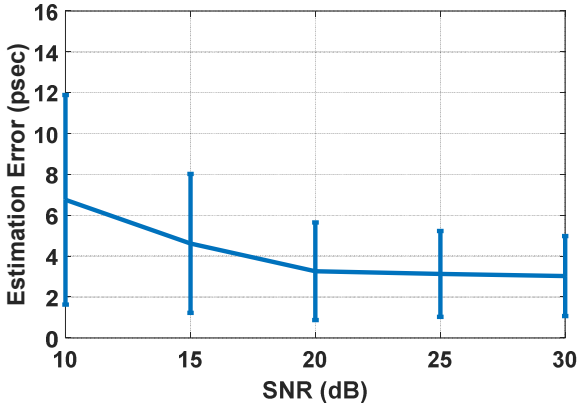


**Fig. 5.** The estimation error versus receiver SNR for $N$=16 antenna elements.

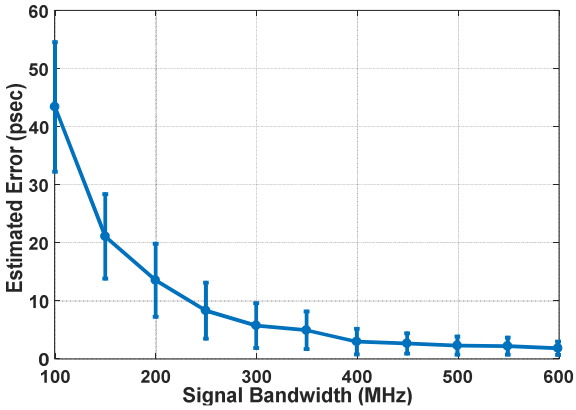


**Fig. 6.** The estimation error versus the signal bandwidth for 30 dB receiver SNR.

As stated in section II, the carrier frequency is not affecting the estimation error, so the relative ambiguity can become significant in higher frequencies. For example at 60 GHz, 3 ps estimation error will result in 18% ambiguity, causing more severe radiation pattern distortion. On the other hand, wider bandwidth is assigned at higher frequencies, so it is important to investigate the performance of the method in variable bandwidth conditions. The bandwidth was varied from 100 MHz to 600 MHz by properly setting the number of the used subcarriers, for $N$=8 and the receiver SNR was set to 30 dB. The results presented in fig. 6, verify that increased bandwidth pro-

vides more accurate estimates of the skew delays. In this sense, the relative ambiguity at higher frequencies can be restricted to acceptable values.

Finally, the radiation pattern distortion of the transmitter antenna array is evaluated. Using a random vector of skew delays for $N$=8 elements, we estimated them and applied the obtained values for compensation. The compensation process is either complete, adding appropriate delays to equalize the propagation time in all cores, or partial, using the method described in [6]. The radiation patterns are depicted in fig. 7. When using the actual delays ranging to hundreds of picoseconds, the radiation patterns coincide with the ones in fig. 7, despite small estimation errors.

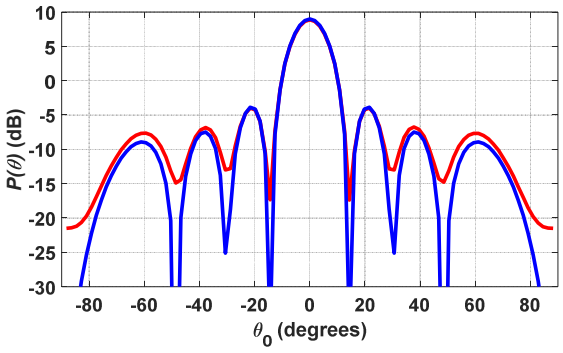


**Fig. 7.** Antenna array factor $P(\theta)$ for $N$=8 elements and receiver SNR= 30 dB, using the estimated delay values in full (blue) and partial (red) compensation methods.

## 4 Conclusion

An accurate and efficient method has been presented for skew estimation in MCF–ARoF beamforming arrangements in multipath propagation environment with variable SNR at the receiver. It can be used for skew compensation after the MCF link is installed, without any prior knowledge of the inter-core differential delays. The method can also be applied more generally, to any RF transmitter employing steerable antenna array, for initial estimation of possible main lobe misalignment and antenna pattern distortion as well as for periodic maintenance. Ongoing work involves the deployment of the ARoF system testbed and the experimental evaluation of the proposed method.

**ACKNOWLEDGMENT** This work was (partly) funded by the EU H2020 blueSPACE (GA No 762055) project.

## References


1. M. Shafi, A. F. Molisch, P. J. Smith, T. Haustein, P. Zhu, P. D. Silva, & G. Wunder, "5G: A tutorial overview of standards, trials, challenges, deployment, and practice", *Journal on Selected Areas in Communications*, vol. 35, no. 6, pp. 1201-1221, 2017.
2. G. Berardinelli, K. Pajukoski, E. Lähetkangas, R. Wichman, O. Tirkkonen, P. E. Mogensen, "On the Potential of OFDM Enhancements as 5G Waveforms", in *79th Vehicular Technology Conference* (*VTC Spring*), pp. 1-5, May 2014.
3. L. Zhuang, C. G. H. Roeloffzen, R. G. Heideman, A. Borreman, A. Meijerink, & W. van Etten, "Single-Chip Ring Resonator-Based 1X8 Optical Beam Forming Network in CMOS-Compatible Waveguide Technology*". IEEE Photonics Technology Letters*, vol. 19, no. 15, pp. 1130-1132, August 2007.
4. T. Nagayama, S. Akiba, T. Tomura, & J. Hirokawa, "Photonics-Based Millimeter-Wave Band Remote Beamforming of Array-Antenna Integrated with Photodiode Using Variable Optical Delay Line and Attenuator", *Journal of Lightwave Technology*, vol. 36, no. 19, pp. 4416-4422, October 2018.
5. B. J. Puttnam, G. Rademacher, R. S. Luís, J. Sakaguchi, Y. Awaji, & N. Wada, "Inter-Core Skew Measurements in Temperature Controlled Multi-Core Fiber", *IEEE 2018 Optical Fiber Communications Conference and Exposition* (*OFC*), pp. 1-3, March 2018.
6. T. Nikas, E. Pikasis, D. Syvridis, "Static Skew Compensation in Multi Core Radio over Fiber systems for 5G Mmwave Beamforming", in *Photonics in Switching and Computing* ( *PSC*), Sept. 2018.
7. M. Eiselt, A. Dochhan, "Single-Ended Fiber Latency Measurement with Picosecond-Accuracy Using Correlation OTDR" *arXiv preprint arXiv:1808.00201*, 2018.
8. D. Hounam, M. Schwerdt, and M. Zink, "Active antenna module characterisation by pseudo-noise gating", in *Proc. 25th ESA Antenna Workshop Satellite Antenna Technol*., Noordwijk, The Netherlands, 2002.
9. B. Brautigam, M. Schwerdt, M. Bachmann, "An efficient method for performance monitoring of active phased array antennas", *IEEE transactions on geoscience and remote sensing*, vol. 47, no. 4, pp. 1236-1243, 2009.